CuO photoelectrodes synthesized by the sol-gel method for water splitting

J. Toupin, H. Strubb, S. Kressmann, V. Artero, N. Krins, Ch. Laberty-Robert

CuO photoelectrodes synthesized by the sol-gel method for water splitting

J. Toupin[a,b], H. Strubb[b], S. Kressman[b], V. Artero[c], N. Krins[a] and Ch. Laberty-Robert[a,*]

[a.] *Sorbonne Universités, UPMC Univ Paris 06, CNRS, Collège de France, Laboratoire de Chimie de la Matière Condensée de Paris, 4 place Jussieu, 75005 Paris.*
[b.] *Total Energies Nouvelles, La Défense, 24 Cours Michelet 92800 Puteaux, France*
[c.] *Laboratoire de Chimie et Biologie des Métaux, Université Grenoble Alpes, CNRS, CEA, 17 rue des Martyrs 38054, Grenoble Cedex 9, France*

* christel.laberty@upmc.fr , +33 (0)1 44 27 56 78

Highlights

- Sol-gel based CuO photoelectrode has values of -0.94 $mA.cm^{-2}$ at pH = 8 and 0 V vs. RHE.
- CuO/TiO_2 photoelectrodes have been synthesized by the sol-gel chemistry coupled with dip-coating.
- These photoelectrodes exhibit -0.5 $mAcm^{-2}$ at pH = 7 and 0 V vs. RHE.
- These photoelectrodes are 100% stable over 600 s.

Abstract

CuO is an attractive photocatalytic material for water splitting due to its high earth abundance and low cost. In this paper, we report the deposition of CuO thin films by sol-gel dip-coating process. Sol deposition has attractive advantages including low-cost solution processing and uniform film formation over large areas with a fairly good control of the film stoichiometry and thickness. Pure CuO phase was obtained for calcination temperatures higher than 360°C in air. The CuO photocurrents for hydrogen evolution depend on the crystallinity and the microstructure of the film. Values of -0.94 $mA.cm^{-2}$ at pH = 8 and 0 V vs. RHE were achieved for CuO photoelectrodes annealed at 400°C under air. More interestingly, the stability of the photoelectrode was enhanced upon the sol-gel deposition of a TiO_2 protective layer. In this all sol-gel CuO/TiO_2 photocathode, a photocurrent of -0.5 $mAcm^{-2}$ is achieved at pH = 7 and 0 V vs. RHE with a stability of ~100% over 600 s.

Keywords : CuO photoelectrode, sol-gel, TiO_2 protecting layer for CuO photoelectrode, water splitting

1. Introduction

The need for clean, safe, and sustainable energy has always been one of the most important challenges for the future, since worldwide energy demand increases continuously. An augmentation of 37% in the next 20 years is indeed envisioned [1]. New energy carriers have to meet severe criteria being renewable, environment-friendly and, high-energy dense. Among the different alternative processes, producing hydrogen fuel directly from inexhaustible sunlight with minimal environment impacts appears to be one of the cleanest and the most advantageous technologies to solve both energy and climate crisis [2, 3].

Photoelectrochemical (PEC) water splitting research was pioneered by Fujishima and Honda in 1972[4], and since this date, many studies have been carried out to find the most efficient semi-conducting materials and the adequate nanostructure to obtain efficient photoelectrode materials. The later must fulfill two criteria: an efficient absorption of sunlight and electronic bands correctly positioned to trigger the water splitting reactions[5]. In addition, they should include components with low toxicity, be earth abundant, and film processing should be low cost as well as easy to scale up[6]. Cost efficiency is of particularly importance since PEC cells need to compete with alternative approaches that consist in wiring traditional photovoltaic panels to commercial water−splitting electrolysers. [7] In this context, photoanode materials should have a band gap of ~ 2.1 eV, a valence band (VB) that is more positive than the apparent potential for oxygen evolution, E^{app} (O_2/H_2O)[5]. These materials must also be stable under oxidative conditions and illumination in aqueous electrolytes. Some metal oxides[8], including TiO_2[9], α-Fe_2O_3[10], WO_3[11], and $BiVO_4$[8a, 12], whose VB consists of O_{2p} orbitals, meet all these requirements. Many p−type semiconductors including GaP, Cu_2O, CuO and p-Si are investigated as photocathode materials for H_2 evolution, as they exhibit adequate band gap comprise between 1.1 to 2.1 eV, and a conduction band (CB) more negative than the apparent potential for H_2 evolution, E^{app}(H_2/H_2O). The stability of photocathode materials in aqueous electrolyte is very important as well.

Based on consideration of cost, earth abundance and electrochemical potential, both Cu_2O and CuO have been identified as promising materials for solar energy conversion [6]. In particular, their conduction band edges are -0.7 V and -0.2 V vs. RHE, respectively [13 14]. Cu_2O is a p−type conductor with a direct band gap of 2 eV [13]. It is thus able to absorb visible light and has a theoretical photocurrent of 14.7 $mA.cm^{-2}$ under standard AM1.5 irradiation. Due to its excellent properties, Cu_2O has been studied by several groups with experimental photocurrents above 7 $mA.cm^{-2}$ in optimized device configurations [15, 16, 17]. CuO is a p−type semiconductor with

a direct band gap of 1.2–1.3 eV, implying that it is theoretically capable of generating a much higher photocurrent of up to 35 mA.cm^{-2}. In comparison to Cu_2O, only very few reports exist on the use of CuO as the active light-harvesting material for photocatalytic water splitting [18,15, 19, 20, 21].

Electrochemical deposition appears to be the most common method used for the formation of Cu_2O thin film photocatalysts [13,16b, 22, 23, 17]. An attractive alternative method that is much less commonly explored is the deposition by dip-coating from sol–gel precursor solutions, followed by thermal annealing. Similar to electrodeposition, sol–gel-based dip-coating deposition presents the advantage to be low cost and scalable. Additionally, a fairly good control of the stoichiometry, film thickness and nanostructure can be achieved. To the extent of our knowledge, there are only few reports on the deposition of CuO thin films by sol-gel process [24, 25, 18].

In this work, we report on the deposition of CuO thin film by dip-coating from sol-gel precursor solutions. We show that pure–phase CuO thin films can be obtained at low temperature. Additionally, we found that the PEC performance of sol–gel deposited CuO thin film strongly depends on the synthesis conditions. Finally, a very thin layer of sol–gel TiO_2 film (100 nm) was deposited onto the best CuO films to enhance the stability of these photoelectrodes. This work not only shows the potential of CuO films as efficient photocathode materials for hydrogen evolution reaction (HER), but also provides an easy, low-cost, and scalable strategy to prepare bi–layer CuO/TiO_2 hydrogen-evolving photoelectrodes for PEC applications.

2. Experimental Section

2.1. CuO photoelectrode synthesis

The CuO films were synthesized by combining dip-coating and sol-gel chemistry, inspired by Ray works [26]. To prepare the copper sol, $CuCl_2.2H_2O$ at 1.5 mol.L^{-1} in methanol was obtained by mixing 1.75 g of $CuCl_2.2H_2O$ in 7 mL of methanol (1.5 M-sol). Dense and mesoporous CuO photoelectrodes with a copper sol at 0.3 mol.L^{-1} have also been investigated (0.3 M-sol). For the synthesis of mesoporous photoelectrode, 90 mg of Poly-iso-butylene-b-polyethylene oxide (Polymer Sources, PIB-*b*-PEO, Mn=7000-*b*-8500) block copolymer dissolved in ethanol/water mixture was first prepared. To this solution, $CuCl_2.2H_2O$ salt was added so that the final concentration in Cu is 0.3 mol.L^{-1}.

The solution previously described is deposited onto FTO substrate (Solems) with a resistivity of 100 Ω.cm^{-1}. Prior to dip-coating, the substrate is cleaned by sonication in ethanol for 5 minutes. The cleaned substrate was then dipped in the sol-gel solution and withdrawn at a speed of 2.5 mm.s^{-1} under dried air (RH = 5-8 %). After dip-coating, the film was treated on a hot-plate at 330°C for 1 min, before being annealed at a temperature comprised between 360°C and 450°C for 30 min to degrade the structuring agent and induce the crystallization of CuO. To increase the total film thickness, several layers were deposited. Between each layer, a treatment under air at 330°C for 1 min was applied to avoid the dissolution of the film during the deposition of the successive layers. This operation was repeated 5 times to reach a thickness of 500 nm (when 1.5 M-sol is used), and of 100 nm (for 0.3M-sol).

2.2. TiO_2 layer synthesis

TiO_2 was deposited using the sol–gel based dip–coating method. [27] First, a Ti5E solution was prepared by mixing 19 g of $TiCl_4$ and 23 g of absolute ethanol. 1mL of this Ti5E solution is then mixed with 5.7 g of absolute ethanol in order to have a concentration of Ti of 0.3 $mol.L^{-1}$ and deposited onto the CuO/FTO substrate with a withdrawal speed of 2.5 mm/s. A heat treatment at 400°C for 1 min under air is applied between each layer (n = 1, 2 or 3) and the final treatment is 500°C for 1 h in air to convert the hybrid organic-amorphous TiO_2 layer into a porous crystalline TiO_2 anatase. The thickness of the TiO_2 layer is ~100 nm for n = 2, evaluated by FE–SEM analysis.

2.3. Characterization of photoelectrodes' microstructure

The morphology of the synthesized films was characterized using a high-resolution scanning electron microscope (Hitachi SU70). XRD patterns were acquired with a Bruker D8 Discover diffractometer in the Bragg-Brentano mode, using Cu Kα radiation (1.540598Å) and a Ni β-filter. Spectra were acquired with a 1D Lynxeye detector from 2θ = 20°– 80° at a step width of 0.05° with acquisition time of 1 s and a source slit width of 4 mm. UV–visible absorption spectra were measured using an Agilent Technologies Cary Series spectrophotometer.

2.4. Photoelectrochemical characterization

The photoelectrochemical performances of the electrodes were evaluated in a three-electrode configuration under front–side light illumination using a Solartron Ametek 2087A Potentiostat / Galvanostat / impedancemeter. The electrolyte was an aqueous solution of Na_2SO_4 (1.0 M) buffered at pH 6 with potassium phosphate (0.1 M). The reference electrode was Ag/AgCl in saturated KCl, and a Pt wire was used as the counter electrode. The photoresponse was measured under chopped irradiation using a 280 W Xe lamp equipped with an ultraviolet filter (Oriel 51272, 400nm) and IR radiation (λ > 950 nm) filter. The light intensity was measured with 1918-R Newport power meter 918D-UVOD3R-UV Silicon Detector (200 – 1100 nm) and estimated to 3 suns (240 $mW.cm^{-2}$, visible-IR irradiation).[28] The scan rate for the linear sweep voltammetry measurements was 20 $mV\ s^{-1}$. Impedance spectroscopy measurements have been performed using the following parameters: frequency range (200 kHz – 0.1 Hz) with a ΔV of 20 mV, at 0 V vs. RHE at pH = 6.

Photocurrent stability tests were carried out by measuring the photocurrent produced under chopped light irradiation (0.1 Hz light/dark cycles frequency) at a fixed potential of 0 V versus RHE.

During linear sweep voltammetry (*j*–V plots) and chronoamperometry (stability plots), the electrolyte was continuously bubbled with N_2 to remove oxygen and thus eliminate erroneous signals arising from oxygen reduction.

3. Results and discussion

The crystalline structure of dense CuO films prepared from 1.5M-sol and calcined at various temperatures has been determined and the results are reported in Fig. 1b. All the diffraction peaks could be indexed as the CuO phase (ICDD card No 801916) and no other impurity peaks are found except those relative to FTO substrate. Additionally, the crystallite size on dense CuO films has been estimated using the Debye-Scherrer formula using

the more intense peak and the deconvolution procedure[29] and the results are reported in Fig. SI1. [30, 31]. The crystallite domains slightly increase with the heat treatment from 63 nm to 71 nm for 360°C and 450°C, respectively.

CuO films are crack-free and relatively dense (Fig.1.a.). They present small particle size, as shown in Fig. 1(a). Upon thermal annealing, the particle size increases. The cross-section SEM images of the CuO films indicate a thickness of approximatively ~ 500 nm for 5 successive layers deposition (not shown).

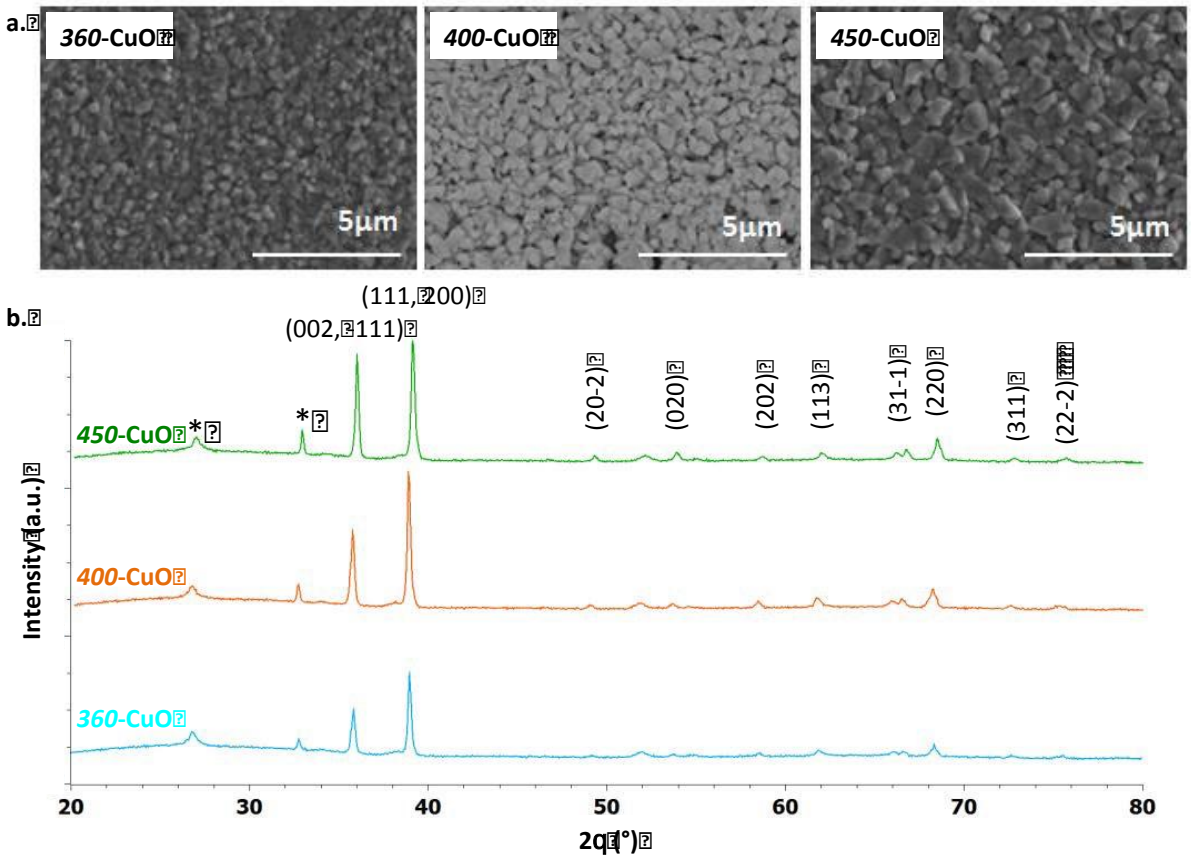

Fig. 1. Characterization of dense CuO photoelectrodes. The films were prepared from the 1.5 M-sol. They were calcined at 360°C for 20 min (*360*-CuO), at 400°C for 20 min (*400*-CuO) and 450°C for 20 min (*450*-CuO): (a) SEM images, (b) X-ray diffractograms. (* indicates SnO_2 from the underlying FTO substrate).

The UV−visible reflectance spectra of dense CuO films are displayed in Fig.2. It can be observed that dense CuO films calcined at 400°C (*400*-CuO) exhibit significantly larger photoabsorption in the visible range than CuO films calcined at 360°C (*360*-CuO) and 450°C (*450*-CuO). This indicates a higher potential for creating electron/hole pairs and potentially enhanced photoelectrochemical performances. The Eg value was estimated from a classical Tauc approach with n = 1, since CuO exhibits a direct band gap transition. The band gap of the *360*-CuO, *400*-CuO and *450*-CuO films is 1.8 e.V, 1.5 e.V. and 1.4 eV, respectively, as shown in Fig. 2.b. The low band gap of *450*-CuO film is attributed to its highest degree of crystallinity, consistent with literature. [32, 33, 34]

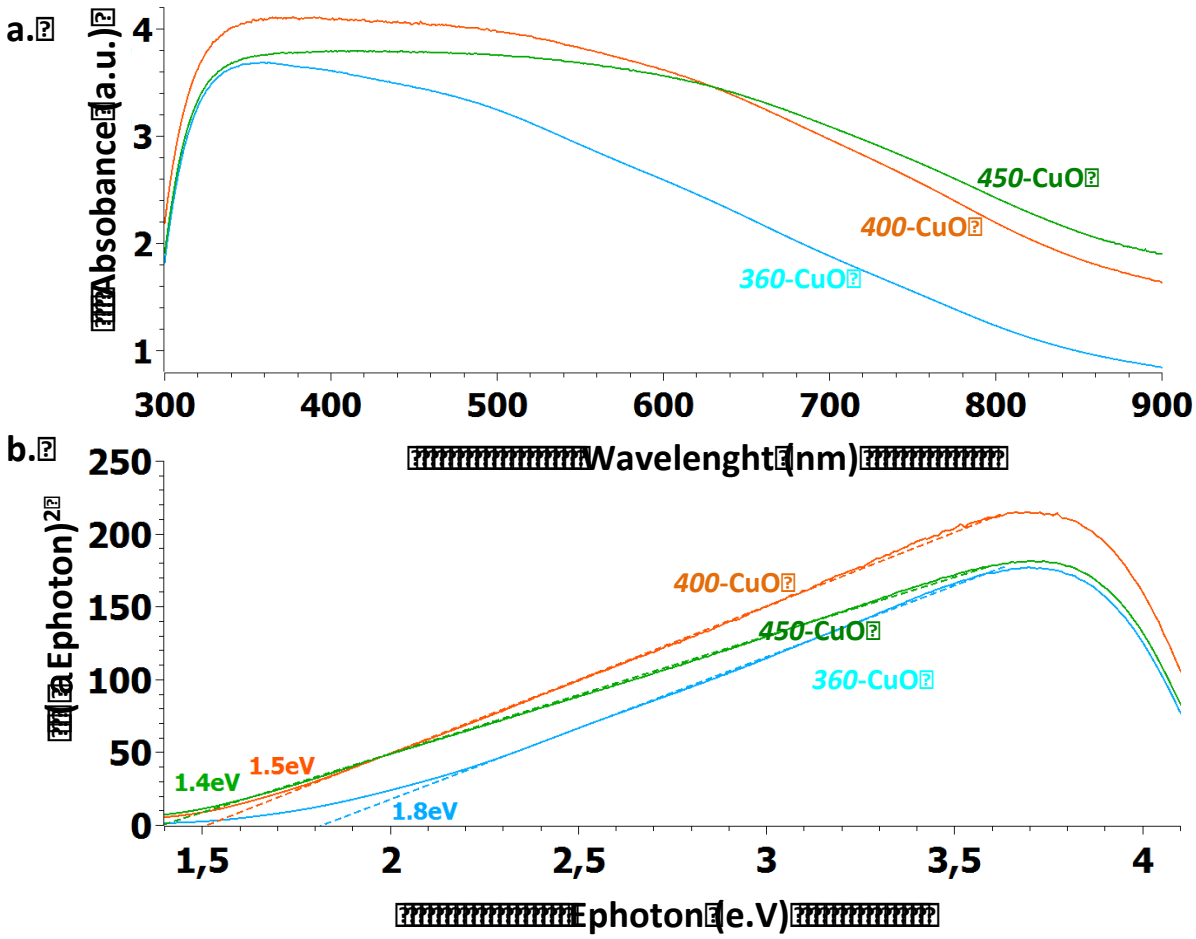

Fig. 2. Optical characterization of dense CuO photoelectrodes. (a) UV–visible diffuse reflectance spectra and (b) Tauc plots $(\alpha E_{photon})^2$ vs. E_{photon}.

The photoelectrochemical performances of dense CuO photocathodes were studied at 0 V vs. RHE and pH = 8 for dense CuO films calcined at various temperatures. The best photocurrent, 0.94 $mA.cm^{-2}$, was obtained for dense CuO films calcined at 400°C (*400*-CuO), indicating that these conditions give rise to the best compromise in terms of light absorption and electrode/electrolyte interface area. The performance of these films is comparable to the one reported by Dass et al. with photocurrents of 1–2 $mA.cm^{-2}$ for 590 nm-thick CuO/$SrTiO_3$ photoelectrodes at -0.9 V. *vs.* SCE (electrolyte, 0.1 M NaOH). [35]

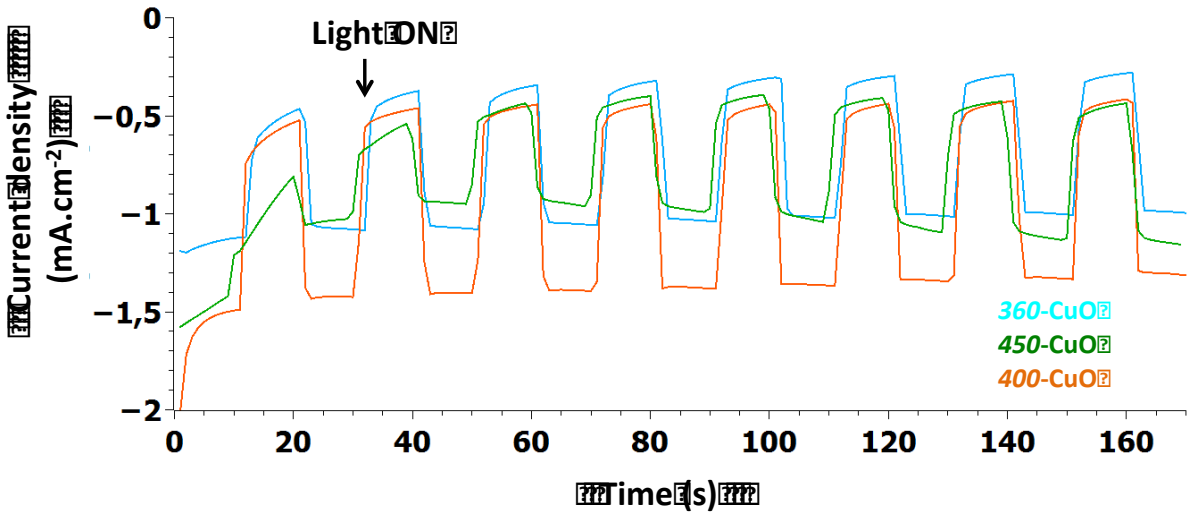

Fig. 3. Photoelectrochemical performances of dense CuO photoelectrodes. Chronoamperometry measurements at 0 V *vs*. RHE and pH = 8 for dense CuO photoelectrodes under chopped visible–light irradiation (3 suns).

Prior to studying the photostability of these CuO photoelectrodes annealed at 400°C, the impact of the nanostructuration onto the photoelectrochemical performances was investigated. To do so, a PIB–*b*–PS block copolymer was used during the preparation of the sol in order to induce porosity during the annealing step. Note that for this study, the sol concentration was 0.3 mol.L^{-1}. The structure and morphology of the mesoporous films annealed at 400 °C for 30 min were studied using X–ray diffraction and FE-SEM, respectively (Fig. SI.2). The X–ray diffraction pattern indicates a pure CuO phase. The surface of the mesoporous film exhibits a network of pores, which is not well organized nor well defined. This poor organization results from the fact that the crystallization of CuO (~ 300°C) occurs after the decomposition of the PIB-*b*-PS block copolymer (~ 200°C) and causes the fragile porous network to collapse. FE–SEM cross–section images on these templated CuO films confirm the very low thickness of the CuO films (~ 100 nm) after the dip-coating of 5 layers. As the film is very thin, the FTO substrate is accessible to the electrolyte through the pores, decreasing the active surface of the film since the FTO substrate does not participate in the H_2 evolution process. The *J-V* curves measured at pH = 6 with a scan rate of 20 mV.s^{-1} for both dense and mesoporous CuO photoelectrodes annealed at 400°C with the same thickness (250 nm) are reported onto Fig. 4. At 0 V *vs*. RHE, the photocurrent is – 0.9 mA.cm^{-2} and – 0.7 mA.cm^{-2} for dense and mesoporous films, respectively. In this specific study, the best result is thus achieved for dense CuO photoelectrodes. This might be explained by i) less electron/hole recombination phenomena because the dense microstructure of the film favours electron/hole transport and ii) reduced light absorption by mesoporous films since their density is lower for similar film thickness.

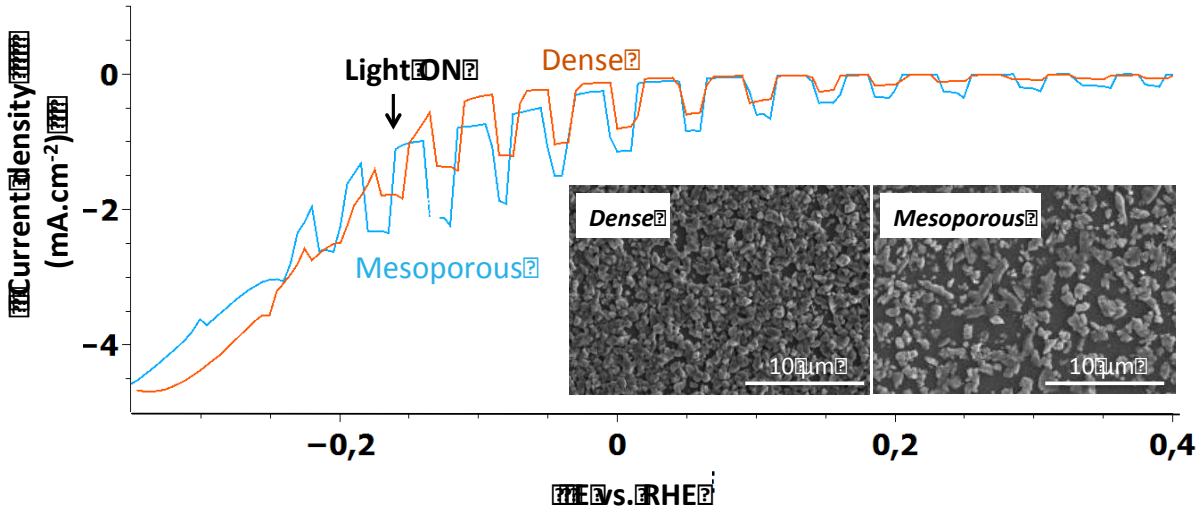

Fig. 4. Impact of the nanostructuration onto PEC properties. *j-V* curves for dense (blue) and mesoporous (orange) CuO films annealed at 400°C for 20 min, obtained from 0.3 M-sol at pH = 6 with a scan rate of 20 mV.s^{-1}. Inset. SEM-FE images of the dense and mesoporous films.

To clarify the origin of the higher photoactivity of dense CuO photoelectrodes, electrochemical impedance spectroscopy (EIS) was employed to investigate the charge transfer rate at the semiconductor/solution interface. Fig. 5 shows the Nyquist plots of the two photocathodes at a potential of 0 V *vs.* RHE measured in the dark (plain mark) and under illumination (open mark). The semicircle features the charge transfer across the semiconductor/electrolyte interface and its diameter represents the charge transfer resistance (Rct). As shown in Fig. 5, Rct decreases upon illumination for the two photocathodes, indicating that illumination accelerates the charge transfer reaction at copper oxide/solution interface due to the photoinduced increase of the carrier density. The dense CuO photoelectrode has the smallest Rct value both in the dark and under illumination, indicating that dense CuO photoelectrodes possess increased charge transfer across the photocathode/solution interface.[36] This might explain why dense CuO electrodes exhibit the best PEC performance for HER. Additionally, UV–visible absorption analyses show a difference in absorption intensity between these two electrodes (Fig. SI3) due to the modification of the film density between dense and mesoporous films.

Altogether, these results highlight that dense CuO films exhibit better electrochemical behavior. This is surprising given the fact that we expect mesoporous films to have better electrochemical behavior because a higher specific surface area. Indeed, a higher electrolyte/semiconductor interface would impact the number of reactive sites and the charge transfer. This indicates that the microstructure of the mesoporous film is not optimized (thickness, porosity network) and that further work is required to optimize the architecture of the mesoporous film for photoelectrochemical properties.

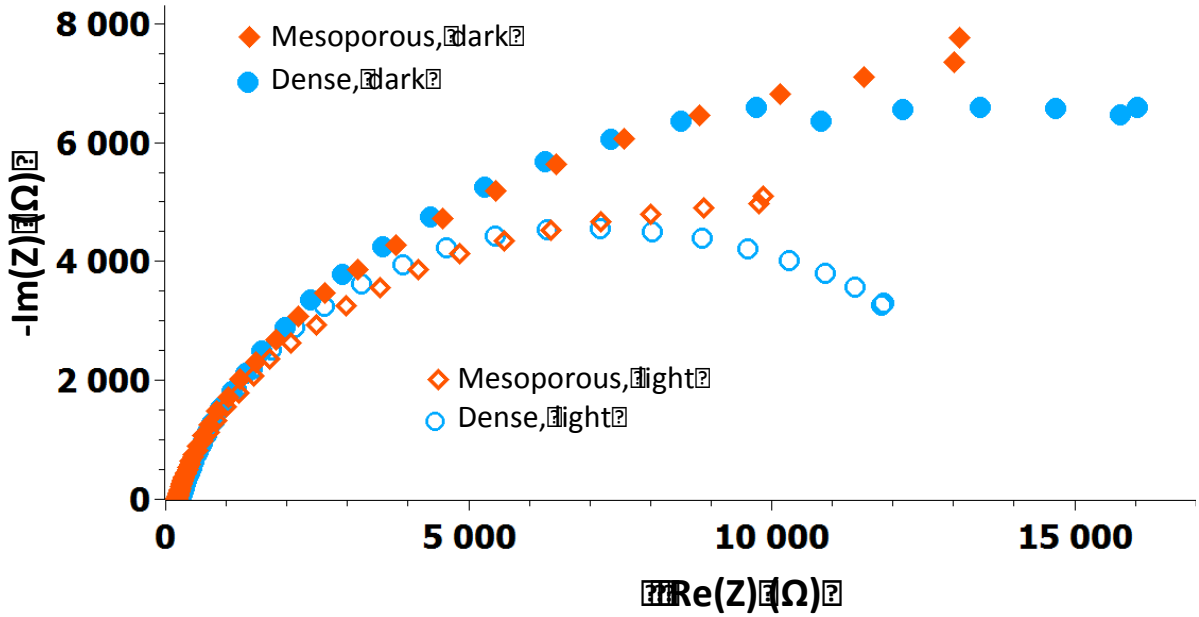

Fig. 5. Nyquist plots measured for the dense and mesoporous CuO photoelectrodes annealed at 400°C (0.3 M-sol) at constant potential of 0 V *vs*. RHE in the dark and under illumination at pH = 6 and 0 V vs. RHE. Measurements from 200 kHz to 0.1 Hz.

A well-known issue of CuO is that it is unstable in aqueous electrolytes.[37] To investigate this, a study of the photocurrent stability of the CuO photocathode was carried out by measuring the current over time at a constant potential of 0 V *vs.* RHE. Over a timescale of 600 s, the drop in photocurrent was about 10% of the initial photocurrent, which suggests that CuO tends to degrade. This is also confirmed by the change of the electrode color occurring during the chronoamperometry test, going from dark grey to orange. Post-mortem XRD analysis of the photoelectrode (Fig. SI4) confirms the formation of metallic copper, due to reductive decomposition of CuO as shown in the following equation:

$$CuO + 2e^- + H_2O \rightarrow Cu° + 2OH^-$$

In order to enhance the stability of CuO photoelectrodes, a thin layer of TiO_2 was deposited on top of *400*–CuO films.[38, 39, 40, 41] This strategy is similar to that reported in our previous work., which showed that substantial improvement of CuO/Cu_2O/FTO photocurrent can be achieved using an anatase TiO_2 layer of 100 nm. [42] The TiO_2 film, deposited using the sol-gel dip-coating approach and annealed at 500°C, is crystalline, which is confirmed with small peaks in the XRD pattern corresponding to the anatase structure (Fig. SI5, a).[27] The intensity of the peaks is low because the thickness of the TiO_2 layer that is very small compared to the CuO photoelectrode. This is confirmed by the SEM images of the bilayer CuO/TiO_2 photoelectrode, where a thickness of 100 nm for TiO_2 layer is measured (*note that this value is achieved for 2 layers of TiO_2 and is 10 times lower than the value observed for CuO*). The absorbance of CuO, TiO_2 and CuO/TiO_2 photoelectrodes were measured and are presented in Fig. S1. The intensity of the absorbance of the CuO photoelectrodes (Figure SI2) solely increases linked to the increase of the amount of matter to absorb photon. Note that no competition exists between the two semiconductor (TiO_2 and CuO); TiO_2 exhibits a band gap superior to 3 eV and CuO of 1.5 eV :TiO_2 absorbs a part of the UV until 350-360 nm, leaving the less energetic photon absorbed by CuO. A possible explanation for the better absorption for the composite electrode containing TiO_2 is related to the difference in

the refractive index between TiO_2 (2.63) and CuO (2.3) that render the reflection less important when TiO_2 is present ontop of CuO. This change in absorbance might increase the number of photogenerated charges. After the formation of CuO/TiO_2 heterojunction, the activity of the electrode decreased while its stability is improved. Fig.6a also shows the variation of the photocurrent density of unprotected CuO electrode and the bi-layers TiO_2/CuO electrode at 0 V vs. RHE at pH = 7. The photocurrent decreases from -1 $mA.cm^{-2}$ for the bare electrode to -0.5 $mA.cm^{-2}$ for the protected CuO photoelectrode at pH = 7 (Fig.6(a)). Concomitantly, the observed onset potential is also impacted (Fig.6(b)) and evolves from 0.4 V vs. RHE to 0.2 V. vs. RHE for CuO and CuO/TiO_2 photoelectrode respectively. The presence of TiO_2 layer ontop of the CuO photoelectrode conduces to a decrease of the photocurrent that might be linked to the presence of defects at the CuO/TiO_2 interface, the change of band bending due to the presence of TiO_2 layer, then favoring the e^-/h recombination. EIS was then performed at the CuO/TiO_2 interface to examine the charge transfer resistance and separation efficiency between the photogenerated electrons and holes. Fig SI.7 shows the typical EIS Nyquist plots under light. We observed a higher resistance for the CuO/TiO_2, accompanied by the higher arc radius of the EIS spectra. This is attributed to the presence of trap states at the CuO/TiO_2 interfaces, hindering photoelectrons.

If after 300 s, the average photocurrent density does not vary for both the protected and the unprotected photoelectrodes, the difference in stability occurs after 600s where the bi-layers TiO_2/CuO retain 100% of initial photocurrent, compared to the unprotected CuO electrode, which suffers a 10% loss. The 100 nm-TiO_2 layer appears to be sufficient to encapsulate the copper oxide photocathodes (Table SI1) and protect them against photoreductive corrosion.

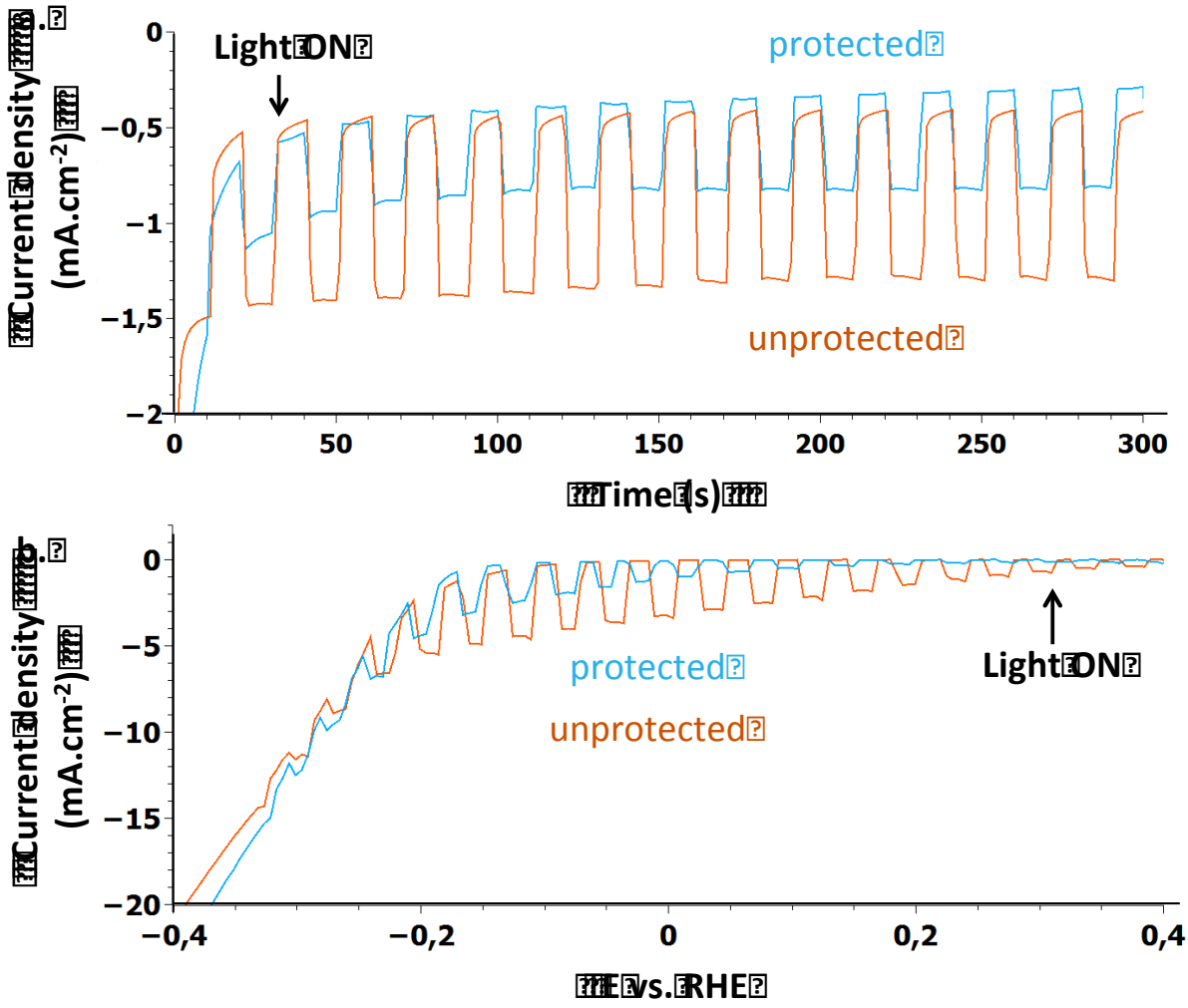

Fig. 6. Unprotected *400*-CuO photoelectrode (orange) and TiO_2-protected *400*-CuO photoelectrode (blue) (a) Chronoamperometry at 0 V *vs.* RHE, (b) *j-V* curves with a scan rate of 20 $mV.s^{-1}$. Both experiments were performed at pH = 7 with light chopped at a frequency of 0.1 Hz.

This result highlights that the protection of CuO photoelectrode by TiO_2 conduces to a decrease of the photocurrent by a factor 2. But, the durability of the electrode is higher for the TiO_2/CuO photoelectrode as 100% of the photocurrent is maintained after 600 s (10 min).

4. Conclusion

Pure CuO thin films have been successfully deposited by a sol-gel dip-coating process. An annealing temperature of 360°C in air was sufficient to obtain the CuO pure phase. When subjected to PEC testing under illumination, the bare CuO photocathodes achieved a maximum of photocurrent of – 0.94 $mA.cm^{-2}$ at 0 V *vs.* RHE for films annealed at 400°C under air. Stability studies indicate a degradation of the CuO photoelectrode over time, corresponding to the reduction of CuO into Cu. The deposition of a TiO_2 protective layer considerably improved the performances of the CuO photoelectrode as 100 % of initial photocurrent was kept over 600 s. This architecture allows

achieving stable photocurrent of $-0.5\ mA.cm^{-2}$ at 0 V vs RHE and pH = 7. Moreover, this work highlights that the strategy of using the sol-gel dip-coating processing followed by a heat–treatment provides an easy, low-cost, and scalable approach to fabricate stable copper-oxide-based materials for hydrogen production. Further work is needed to develop mesoporous films with higher performances for photoelectrochemical application. For example, a systematic study where the thickness of the film is optimized as a function of the porosity will be necessary.

Notes

Electronic supplementary material: The online version of this article (https://doi.org/10.1007/s10971-017-4519-4) contains supplementary material, which is available to authorized users.

Acknowledgements: This work was supported by the ANRT, the Agence Nationale de la Recherche through the LabEx ARCANE programme (ANR-11-LABX-0003-01) and Total-Energie Nouvelle.

Conflict of interest. The authors declare that there is no conflict of interest.

References

1. Dudley, B., BP Energy Outlook 2035. *BP's Energy Outlook* **2014**, 94.
2. Lewis, N.S., Nocera, D. G. L., Powering the planet: chemical challenges in solar energy utilization. *PNAS* **2006,** *103* (43), 15729-15735.
3. Yilanci, A., Dincer, I.; Ozturk, H.K., A review on solar-hydrogen/fuel cell hybri energy systems for stationary applications. *Prog. Energy Combust.Sci.* **2009,** *35* (3), 231-244.
4. Fujishima, A., Honda, K., Electrochemical Photolysis of water at a semiconductor electrode. *Nature* **1972,** *238*, 37-38.
5. Van de krol, R., Principles of Photoelectrochemical cells. In *Photoelectrochemical Hydrogen Production. Electronic Materials: Science & Technology*, van de Krol R., G. M., Ed. Springer, Boston, MA: Boston, 2012; Vol. 102, pp 13-67.
6. Wadia, C., Alivisatos, A.P., Kammen, D. M., Materials Availability Expands the Opportunity for Large-Scale Photovoltaics Deployment. *Environ. Sci. Technol.* **2009,** *43* (6), 2072-2077.
7. Dincer, I., Technical, environmental and exergetic aspects of hydrogen energy systems. *Int J Hydrogen Energ* **2002,** *27* (3), 265-285.
8. (a) Bhat, S. S. M.; Jang, H. W., Recent Advances in Bismuth-Based Nanomaterials for Photoelectrochemical Water Splitting. *Chemsuschem* **2017,** *10* (15), 3001-3018; (b) Abdi, F. F.; Berglund, S. P., Recent developments in complex metal oxide photoelectrodes. *J. Phys. D-Appl. Phys.* **2017,** *50* (19), 22.
9. Courtin, E.; Baldinozzi, G.; Sougrati, M. T.; Stievano, L.; Sanchez, C.; Laberty-Robert, C., New Fe2TiO5-based nanoheterostructured mesoporous photoanodes with improved visible light photoresponses. *Journal of Materials Chemistry A* **2014,** *2* (18), 6567-6577.
10. (a) Hamd, W.; Cobo, S.; Fize, J.; Baldinozzi, G.; Schwartz, W.; Reymermier, M.; Pereira, A.; Fontecave, M.; Artero, V.; Laberty-Robert, C.; Sanchez, C., Mesoporous alpha-Fe2O3 thin films synthesized via the sol-gel process for light-driven water oxidation. *Physical Chemistry Chemical Physics* **2012,** *14* (38), 13224-13232; (b) Iandolo, B.; Wickman, B.; Zoric, I.; Hellman, A., The rise of hematite: origin and strategies to reduce the high onset potential for the oxygen evolution reaction. *Journal of Materials Chemistry A* **2015,** *3* (33), 16896-16912; (c) Sivula, K.; Le Formal, F.; Gratzel, M., Solar Water Splitting: Progress Using Hematite (alpha-Fe2O3) Photoelectrodes. *Chemsuschem* **2011,** *4* (4), 432-449.
11. Hilliard, S.; Baldinozzi, G.; Friedrich, D.; Kressman, S.; Strub, H.; Artero, V.; Laberty-Robert, C., Mesoporous thin film WO3 photoanode for photoelectrochemical water splitting: a sol-gel dip coating approach. *Sustainable Energy & Fuels* **2017,** *1* (1), 145-153.
12. (a) Hilliard, S.; Friedrich, D.; Kressman, S.; Strub, H.; Artero, V.; Laberty-Robert, C., Solar-Water-Splitting BiVO4 Thin-Film Photoanodes Prepared By Using a Sol-Gel Dip-Coating Technique. *ChemPhotoChem* **2017,** *1* (6), 273-280; (b) Song, J.; Cha, J.; Lee, M. G.; Jeong, H. W.; Seo, S.; Yoo, J. A.; Kim, T. L.; Lee, J.; No, H.; Kim, D. H.; Jeong, S. Y.; An, H.; Lee, B. H.; Bark, C. W.; Park, H.; Jang, H. W.; Lee, S., Template-engineered epitaxial BiVO4 photoanodes for efficient solar water splitting. *Journal of Materials Chemistry A* **2017,** *5* (35), 18831-18838.
13. Paracchino, A.; Laporte, V.; Sivula, K.; Gratzel, M.; Thimsen, E., Highly active oxide photocathode for photoelectrochemical water reduction. *Nat Mater* **2011,** *10* (6), 456-461.
14. Yoon, S. K., M.; Kim, I.S.; Lim, J.H.; Yoo, B., Manipulation of cuprous oxide surfaces for improving their photocatalytic activity. *J. Mater. Chem. A.* **2014,** *2*, 11621-11627.
15. Lin, C. Y., Lai, Y.H.; Mersch, D.; Reisner, E., Cu2O|NiOx nanocomposite as an inexpensive photocathode in photoelectrochemical water splitting. *Chem. Sci.* **2012,** *3*, 3482-3487.
16. (a) Paracchino, A.; Brauer, J. C.; Moser, J. E.; Thimsen, E.; Graetzel, M., Synthesis and Characterization of High-Photoactivity Electrodeposited Cu2O Solar Absorber by Photoelectrochemistry and Ultrafast Spectroscopy. *Journal of Physical Chemistry C* **2012,** *116* (13), 7341-7350; (b) Zhang, Z., Wang, P. , Highly stable copper oxide composite as an effective photocathode for water splitting via a facile electrochemical synthesis strategy. . *J. Mater. Chem.* **2012,** *22*, 2456
17. Zhang, Z., Dua R., Zhang L., Zhu H., Zhang H., Wang P., Carbon-Layer-Protected Cuprous Oxide Nanowire Arrays for Efficient Water Reduction. . *ACS Nano* **2013,** *7*, 1709-1717.

18. Lim, Y. F., Chua, C. S., Lee, C. J., Chi, D. , Sol-gel deposited Cu2O and CuO thin films for photocatalytic water splitting. . *Phys. Chem. Chem. Phys.* **2014,** *16*, 25928–25934
19. Jin, Z., Zhang, X., Li, Y., Li, S. & Lu, G. , 5.1% Apparent quantum efficiency for stable hydrogen generation over eosin-sensitized CuO/TiO2 photocatalyst under visible light irradiation. . *Catal. Commun.* **2007,** *8*, 1267–1273
20. Liu, Z. B., H.; Xu, S.; Sun, D.D., Hierarchical CuO/ZnO "corn-like" architecture for photocatalytic hydrogen generation. *Int J Hydrogen Energ* **2011,** *36* (21), 13473-13480.
21. Pai, Y. H. F., Fang, S.Y., Preparation and characterization of porous Nb2O5 photocatalysts with CuO, NiO and Pt cocatalyst for hydrogen production by light-induced water splitting. *Journal of Power Sources* **2013,** *230*, 321-326.
22. Paracchino, A., Mathieu, N., Hisatomi, T., Stefik, M., Tilley, S.D.; Graetzel, M., Ultrathin films on copper(I) oxide water splitting photocathodes: a study on performance and stability. *Energy & Environmental Science* **2012,** (5), 8673-8681.
23. Morales-Guio, C. G.; Tilley, S. D.; Vrubel, H.; Gratzel, M.; Hu, X. L., Hydrogen evolution from a copper(I) oxide photocathode coated with an amorphous molybdenum sulphide catalyst. *Nat Commun* **2014,** *5*.
24. Hench, L., Hench, West, J.K., The sol-gel process. *Chem. Rev.* **1990,** *90* (1), 33-72.
25. Jia, Q. X., McCleskey M., T.M., Burrell, A.K.; Lin, Y., Collis, G.E., Wang, H., Li, Q, Foltyn, S.R., Polymer-assisted deposition of metal-oxide films. *Natture Materials* **2004,** *3*, 529-532.
26. Ray, S. C., Preparation of copper oxide thin film by the solègel like dip technique and study of their structural and optical properties. *Sol. Energy Mater. & Solar Cells* **2001,** *68* (3-4), 307-312.
27. Grosso, D.; Soler-Illia, G.; Crepaldi, E. L.; Cagnol F, F.; Sinturel C, C.; Bourgeois, A.; Brunet-Bruneau, A.; Amenitsch, H.; Albouy, P. A.; Sanchez, C. N., Highly porous TiO2 Anatase optical thin films with cubic mesostructure stabilised at 700°C. *Chemistry of Materials* **2003,** *15* (24), 4562.
28. Under such conditions, the photocurrent is threefold enhanced with regards to solar irradiation.
29. Patterson, A. L., The scherrer formula for X-ray particle size determination. *Phys. Rev.* **1939,** *56* (10), 978-982.
30. Koshy, J., Goerge, K.C., Annealing effects on crystallite size and band gap of CuO nanoparticles. *International Journal Nanoscience Nanotechnology* **2015,** *6* (1), 1-8.
31. Habibi, M. H., Bahareh B., Effect of annealing temperature on crystalline phase of copper oxide nanoparticle by coppe acetate precursor and sol-gel method. *J. Therm. Anal. Calorim.* **2014,** *115* (1), 419-423.
32. Nakaoka, K., Ueyama, J., Ogura, K., Photoelectrochemical Behavior of Electrodeposited CuO and Cu2O Thin Films on Conducting Substrates. . *J. Electrochem. Soc.* **2004,** *151*, C661–C665.
33. Kidowaki, H. O., T.; Akiyama, T.; Suzuki, A.; Jeyadevan, B.; Cuya, J., Fabrication and Characterization of CuO-based solar cells. *J. Mater. Sci. Res.* **2012,** *1* (1), 138-143.
34. Johan, M. R., Suan M.S.M, Hawari, N.L., Ching, H.A., Annealing effects on the properties of copper oxide thin films prepared by chemical deposition. *Int. J. Electrochem. Sci.* **2011,** *6*, 6094-6104.
35. Surbhi Choudhary, A. S., Sumant Upadhyay, Nirupama Singh, Vibha R. Satsangi, Rohit Shrivastav, Sahab Dass Nanostructured CuO/SrTiO3 bilayered thin films for photoelectrochemical water splitting. *Journal of Solid State Electrochemistry* **2013,** *17* (9), 2531–2538.
36. Zhang, Z. H.; Wang, P., Highly stable copper oxide composite as an effective photocathode for water splitting via a facile electrochemical synthesis strategy. *Journal of Materials Chemistry* **2012,** *22* (6), 2456-2464.
37. Ma, Q.-B.; Hofmann, J. P.; Litke, A.; Hensen, E. J. M., Cu2O photoelectrodes for solar water splitting: Tuning photoelectrochemical performance by controlled faceting. *Solar Energy Materials and Solar Cells* **2015,** *141*, 178-186.
38. Siripala, W.; Ivanovskaya, A.; Jaramillo, T. F.; Baeck, S.-H.; McFarland, E. W., A Cu2O/TiO2 heterojunction thin film cathode for photoelectrocatalysis. *Solar Energy Materials and Solar Cells* **2003,** *77* (3), 229-237.
39. Rokhmat, M.; Wibowo, E.; Sutisna; Khairurrijal; Abdullah, M., Performance Improvement of TiO2/CuO Solar Cell by Growing Copper Particle Using Fix Current Electroplating Method. *Procedia Engineering* **2017,** *170* (Supplement C), 72-77.

40. Zainun, A. R.; Tomoya, S.; Mohd Noor, U.; Rusop, M.; Masaya, I., New approach for generating Cu2O/TiO2 composite films for solar cell applications. *Materials Letters* **2012,** *66* (1), 254-256.
41. Wang, P.; Wen, X.; Amal, R.; Ng, Y. H., Introducing a protective interlayer of TiO2 in Cu2O-CuO heterojunction thin film as a highly stable visible light photocathode. *RSC Advances* **2015,** *5* (7), 5231-5236.
42. Toupin, J.; Strub, H. P.; Kressmann, S.; Boudot, M.; Artero, V.; Laberty, C., Engineering n-p junction for photo-electrochemical hydrogen production. *Physical Chemistry Chemical Physics* **2017**.